


Electronic excited states from a variance-based contracted quantum eigensolverYuchen Wang  and David A. Mazziotti **Department of Chemistry and The James Franck Institute, The University of Chicago, Chicago, Illinois 60637, USA* (Received 6 May 2023; revised 10 July 2023; accepted 9 August 2023; published 25 August 2023)

Electronic excited states of molecules are central to many physical and chemical processes, and yet they are typically more difficult to compute than ground states. In this paper we leverage the advantages of quantum computers to develop an algorithm for the highly accurate calculation of excited states. We solve a contracted Schrödinger equation (CSE)—a contraction (projection) of the Schrödinger equation onto the space of two electrons—whose solutions correspond identically to the ground and excited states of the Schrödinger equation. While recent quantum algorithms for solving the CSE, known as contracted quantum eigensolvers (CQEs), have focused on ground states, we develop a CQE based on the variance that is designed to optimize rapidly to a ground or excited state. We apply the algorithm to compute the ground and excited states of H_2 , H_4 , and BH.

DOI: [10.1103/PhysRevA.108.022814](https://doi.org/10.1103/PhysRevA.108.022814)**I. INTRODUCTION**

Electronic excited states of molecules are critically important in any physical or chemical process that is not confined to the ground state such as photoabsorption and emission [1], nonadiabatic dynamics [2,3], and electron scattering and transport [4,5]. Despite their central importance, excited states are more difficult to compute than ground states [6,7]. Typical approaches compute the excited states as a response to the ground state [8–12], which has limitations whenever excited states differ substantially from the ground state, e.g., in double- or multi-excitation processes [13], charge-transfer states [14,15], core excitations [16], Rydberg states [17], as well as conical intersections [18,19].

One promising direction is to harness the potential advantages of quantum computers [20,21]. In the absence of noise, quantum computers can prepare and measure quantum states whose wave functions are challenging to represent and manipulate on classical devices, potentially realizing significant advantages relative to classical devices [22]. While recent molecular algorithms have primarily focused on computing ground states [21] or obtaining multiple excited states at once from response theory [23–27] or a Krylov expansion [23,28–44], quantum computers may be particularly well suited to realizing more accurate and direct calculations of excited states. The possible advantages for ground states are, in principle, amplified for excited states, which are often formed from excitations to degenerate orbitals that produce significant multireference correlation even when the ground state is minimally correlated.

In this paper we develop an algorithm for the highly accurate state-specific calculation of excited states on quantum devices. Consider the contraction of the Schrödinger equation onto the space of two electrons, known as the contracted Schrödinger equation (CSE) [45–49]. The CSE has two signif-

icant properties: (i) its solutions correspond identically to the ground- and excited-state solutions of the Schrödinger equation [45,46], and (ii) its compact structure reveals an exact two-body exponential parametrization of both ground and excited states [50,51]. Recent quantum-computing algorithms for solving the CSE or a part of the CSE, known as contracted quantum eigensolvers (CQEs) [52–57], have mainly focused on the ground state. We develop a CQE based on the energy variance that is designed to optimize rapidly to a ground or excited state. Using the CSE has a potential advantage over other variance-based approaches [58–63] because considering the CSE in addition to the variance provides a compact, exact ansatz for the wave function as a product of two-body transformations [50,51]. Moreover, the product form of this ansatz allows us to obtain exact results in the absence of noise from optimizing only the parameters introduced in the current iteration while variational methods—even those that use an ansatz like the anti-Hermitian contracted Schrödinger equation (ACSE) such as the adaptive variational quantum eigensolver—require optimization of all parameters in the calculation. To demonstrate, we apply the algorithm to computing the ground and excited states of H_2 , H_4 , and BH.

II. THEORY

For a many-electron system consider the Schrödinger equation

$$(\hat{H} - E_n)|\Psi_n\rangle = 0 \quad (1)$$

in which \hat{H} is the Hamiltonian operator and $|\Psi_n\rangle$ is the N -electron wave function for the n th state. The CSE projects the Schrödinger equation onto all two-electron transitions [45–49,52]:

$$\langle\Psi_n|\hat{a}_i^\dagger\hat{a}_j^\dagger\hat{a}_l\hat{a}_k(\hat{H} - E_n)|\Psi_n\rangle = 0, \quad (2)$$

where \hat{a}_i^\dagger and \hat{a}_i are the creation and the annihilation operators for the i th orbital. As proved by Nakatsuji [64] in first

*damazz@uchicago.edu

quantization and one of the authors [45] in second quantization, the CSE is satisfied by a wave function $|\Psi_n\rangle$ if and only if it satisfies the Schrödinger equation. The proofs show that the CSE implies the energy variance which implies the Schrödinger equation. Hence, the CSE determines a set of ground and excited states that is identical to that of the Schrödinger equation.

As shown previously, the CSE can be solved for the ground-state wave function by minimizing the following energy functional iteratively on a quantum computer [52–57]:

$$\min_{^2F_m} E[{}^2F_m], \quad (3)$$

where

$$E[{}^2F_m] = \langle \Psi_m | \hat{H} | \Psi_m \rangle, \quad (4)$$

in which

$$|\Psi_m\rangle = e^{\hat{F}_m} |\Psi_{m-1}\rangle \quad (5)$$

and

$$\hat{F}_m = \sum_{pqst} {}^2F_m^{pq:st} \hat{a}_p^\dagger \hat{a}_q^\dagger \hat{a}_t \hat{a}_s. \quad (6)$$

The \hat{F}_m is the two-body operator in the exponential transformation of the wave function at the m th iteration, and 2F_m is the two-body transformation matrix, defining \hat{F}_m in Eq. (6) where its elements are explicitly denoted by ${}^2F_m^{pq:st}$. This wave function is the CSE ansatz with the special property that its iterative minimization with respect to each two-body operator \hat{F}_m converges to an exact solution of the CSE and, hence, an exact solution of the Schrödinger equation within a given finite basis set [50,51]. The gradient of the energy with respect to the latest 2F_m is the residual of the CSE. Hence, the gradient vanishes if and only if the CSE is satisfied. We can also implement subsets of the CSE ansatz on a quantum computer. For example, we have restricted the two-body operators \hat{F}_m to be anti-Hermitian which generates strictly unitary transformations [52–56]. In this case the vanishing of the gradient causes the anti-Hermitian part of the CSE, known as the ACSE [48,49,65–68], to be satisfied.

To extend to excited states, we replace the iterative minimization of the energy by an iterative minimization of the energy variance:

$$\min_{^2F_m} \text{Var}[{}^2F_m], \quad (7)$$

where

$$\text{Var}[{}^2F_m] = \langle \Psi_m | (\hat{H} - E_m)^2 | \Psi_m \rangle, \quad (8)$$

in which

$$E_m = \langle \Psi_m | \hat{H} | \Psi_m \rangle, \quad (9)$$

with the wave function given by the CSE ansatz in Eq. (5) and the two-body operator \hat{F}_m and transformation matrix 2F_m defined in Eq. (6). Throughout we assume that the wave function $|\Psi_m\rangle$ has been renormalized to one if necessary. While the excited states are saddle points of the energy, they are minima of the variance. Moreover, any minimum is an exact stationary-state solution of the Schrödinger equation (and the

CSE) if the variance vanishes. The variance has recently been applied for excited states in the context of the variational quantum eigensolver [58–63]; however, in these studies the variance is not used to determine the variational ansatz for the wave function. Here we use the CSE, which implies the variance [45,64], to not only perform the optimization but also to determine the iterative structure of the wave function via Eq. (5). The CSE ansatz is formally exact with the important property that it remains exact even without reoptimization of the ${}^2F_{m-q}$ for $q > 0$ from previous iterations. Assuming that the Hamiltonian and wave function are real, the gradient of the variance with respect to 2F_m evaluated in the limit that ${}^2F_m = 0$ can be computed as follows:

$$\frac{\partial \text{Var}}{\partial ({}^2F_m^{st:pq})} = 2 \langle \Psi_{m-1} | (\hat{\Gamma}_{st}^{pq} - {}^2D_{st}^{pq})(\hat{H} - E_{m-1})^2 | \Psi_{m-1} \rangle, \quad (10)$$

in which $\hat{\Gamma}_{st}^{pq} = \hat{a}_p^\dagger \hat{a}_q^\dagger \hat{a}_t \hat{a}_s$ and the elements of the two-particle reduced density matrix (2-RDM) are

$${}^2D_{st}^{pq} = \langle \Psi_{m-1} | \hat{\Gamma}_{st}^{pq} | \Psi_{m-1} \rangle. \quad (11)$$

Practically, we can approximate the minimization of the variance at the m th iteration by selecting 2F_m to be proportional to the direction of the gradient or a related search direction from any gradient-descent method with the proportionality constant (or step size) being determined by a line search. Other related generalizations of the variational principle in the CQE can also be considered. For example, we can (1) solve the CSE or ACSE directly for the wave function, (2) minimize the least-squares norm of the CSE or ACSE, or (3) augment the variance functional with an additional functional such as a small amount of the energy functional.

Optimizing the energy variance is ideal for a quantum computer. While computing the variance requires not only the two-particle reduced density matrix (2-RDM) but also the four-particle RDM on a classical computer, we can readily compute it at the m th iteration on a quantum computer by introducing an ancillary qubit to generate the extra wave function

$$|\tilde{\Psi}_m\rangle = e^{i\delta(\hat{H}-E_m)} |\Psi_m\rangle \quad (12)$$

such that

$$\langle \Psi_m | (\hat{H} - E_m)^2 | \Psi_m \rangle \approx \frac{1 - \text{Re} \langle \Psi_m | \tilde{\Psi}_m \rangle}{\delta^2/2}, \quad (13)$$

where $\text{Re}(z)$ returns the real part of z , the approximation is accurate to $O(\delta^2)$, and δ is a small parameter. The schematic circuit diagram in Fig. 1 shows how we can use the ancillary qubit to prepare an entangled state of the two wave functions whose tomography can yield the overlap between the two states. This formula is an extension of the difference formulas employed in previous CQE algorithms [52] as well as in the context of open quantum systems [69]. As shown in previous work, the limit of δ approaching zero can be computed by using Richardson's extrapolation from a series of δ values [69,70].

Recently, we have shown how the residuals of both the CSE and ACSE can be efficiently calculated on a quantum

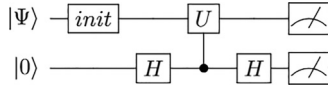


FIG. 1. We first prepare the initial state $|\Psi_m\rangle$ on the main qubits and apply the Hadamard gate to the ancillary qubit to generate $(|0\rangle \otimes |\Psi\rangle + |1\rangle \otimes |\Psi\rangle)/\sqrt{2}$. We then apply a controlled unitary operation that generates the extra wave function $|\tilde{\Psi}_m\rangle$ in Eq. (12) when the ancillary qubit is 1 to produce $(|0\rangle \otimes |\Psi_m\rangle + |1\rangle \otimes |\tilde{\Psi}_m\rangle)/\sqrt{2}$. Applying a second Hadamard gate to the ancillary qubit yields $(|0\rangle \otimes |\Psi_m + \tilde{\Psi}_m\rangle + |1\rangle \otimes |\Psi_m - \tilde{\Psi}_m\rangle)/2$. Measuring the ancillary qubit in the z basis $\langle\sigma_z\rangle$ gives the real part of the overlap $\text{Re}(\langle\Psi_m|\tilde{\Psi}_m\rangle)$ that allows us to compute the variance as in Eq. (13) [71].

computer from only a 2-RDM-like tomography [52,57]. Similarly, the key term in the gradient of the variance with respect to 2F in the CSE wave-function ansatz can be computed from a 2-RDM-like tomography:

$$\langle\Psi_m|\hat{\Gamma}_{st}^{pq}(\hat{H} - E_m)^2|\Psi_m\rangle \approx \frac{2D_{st}^{pq} - \text{Re}(\langle\Psi_m|\hat{\Gamma}_{st}^{pq}|\tilde{\Psi}_m\rangle)}{\delta^2/2}, \quad (14)$$

where the approximation is accurate to $O(\delta^2)$. While the left side formally depends on the six-particle RDM, through a combination of state preparation and tomography, we can obtain the gradient of the variance with the CSE ansatz from only the measurement of the two-particle reduced transition matrix between the states $|\Psi_m\rangle$ and $|\tilde{\Psi}_m\rangle$. Because of the ancillary qubit, the tomography of the 2-RDMs of each state as well as their two-particle reduced transition matrix can be performed by standard techniques—measuring the two-particle expectation values expressed as Pauli strings, as discussed in previous work [52,57], although more advanced sampling techniques like shadow tomography [72] could also be employed. The circuit to generate the state for measuring the two-particle reduced transition matrix is similar to that given in Fig. 1 for the transition overlap in the variance. Formulas in Eqs. (13) and (14) assume that the Hamiltonian and wave function are real, but as in Refs. [52,69], they can be readily generalized through additional measurements to treat complex Hamiltonians and wave functions as well as to realize higher-order approximations. The algorithm for the variance-based CQE for excited states is summarized in Table I. In Step 5 we compute the gradient descent direction \hat{F}_{m+1} which can be

TABLE I. Variance-based CQE algorithm.

Algorithm: Variance-based CQE

- Given $m = 0$ and convergence tolerance ϵ .
 Choose initial wave function $|\Psi_0\rangle$.
 Repeat until the energy variance is less than ϵ .
 Step 1: Prepare $|\tilde{\Psi}_m\rangle = e^{i\delta(\hat{H}-E_m)}|\Psi_m\rangle$
 Step 2: Measure variance using Eq. (13)
 Step 3: Measure $\langle\Psi_m|\hat{a}_p^\dagger\hat{a}_q^\dagger\hat{a}_i\hat{a}_s|\tilde{\Psi}_m\rangle$ in Eq. (14)
 Step 4: Compute gradient from Eqs. (10) and (14)
 Step 5: Compute gradient-descent search direction \hat{F}_{m+1}
 Step 6: Prepare $|\Psi_{m+1}\rangle = e^{\hat{F}_{m+1}}|\Psi_m\rangle$
 Step 7: Optimize magnitude of \hat{F}_{m+1} via Steps 1, 2, and 6
 Step 8: Set $m = m + 1$
-
-

the gradient, as in Eq. (14), or a second-order update from a conjugate gradient or quasi-Newton method [73]; in Step 7 we optimize the magnitude of \hat{F}_{m+1} by performing a line search along the descent direction.

III. APPLICATIONS

After a discussion of the methodology in Sec. III A, we present the results from the excited-state CQE algorithm in Sec. III B.

A. Methodology

To demonstrate, we apply the variance-based CQE algorithm to computing the excited states of the molecules H_4 , BH, and H_2 . Both BH and H_4 are solved classically with all unitary transformations performed with respect to a wave function that is represented by a vector. These calculations demonstrate the algorithm in the absence of either noise or sampling errors. We also compute the excited states of H_2 which is simulated in Qiskit [74] using both a state-vector simulator without noise or sampling errors as well as a simulator with a Qiskit noise model that reproduces the errors of the IBM quantum computer Lagos. We encode the fermionic molecular H_2 Hamiltonian onto four qubits through the Jordan-Wigner mapping [75]. After decomposing the operators in the Pauli basis, we implement the unitary propagators by first-order Trotter expansions. The addition of a fifth, ancillary qubit allows us to measure the transition overlap and the two-particle transition matrix in Eqs. (13) and (14), respectively. We measure the 2-RDM and two-particle transition matrix by standard techniques where the fermionic operators are expressed as Pauli strings [52,57]. The fake-Lagos simulator employs 8192 shots for its measurements.

The H_4 molecule is treated in its linear conformation with adjacent hydrogen atoms separated by 1 Å. We use a minimal Slater-type orbital (STO-3G) basis set [76] for H_2 and an STO-6G basis set for H_4 and BH as well as a frozen $1s$ core for the boron atom in BH. Molecular orbitals from the Hartree-Fock method and one- and two-electron integrals are obtained with the Quantum Chemistry Package in Maple [77]. In implementing the algorithm in Table I, we restrict the \hat{F} operators to be anti-Hermitian, making the two-body exponential transformations unitary. For H_2 we use the gradient for the gradient-descent direction in Step 5 and determine the magnitude of the \hat{F}_{m+1} in Step 7 from a fixed step ϵ along the gradient with $\epsilon = 0.15$ for the state-vector and fake-Lagos simulators, but for H_4 and BH we compute a quasi-second-order gradient descent direction in Step 5 from a limited-memory Broyden–Fletcher–Goldfarb–Shanno (BFGS) method [73] and determine the magnitude of the \hat{F}_{m+1} in Step 7 from an exact line search. The δ parameter in Step 1 and Eqs. (13) and (14) is taken in the infinitesimal limits for the classical and state-vector simulations while it is set to a finite value $\delta = 0.01$ for the fake-Lagos simulator to distinguish the measured change from the noise.

Initial guesses for the wave function are the Slater determinants from the Hartree-Fock orbitals; when $\langle\hat{S}_z\rangle = \pm 1$, we

TABLE II. The energy, energy error, variance, and least-squares CSE norm of the ground state and each of the first 15 excited states of linear H_4 from the variance-based CQE are shown. Energies are given in hartrees.

State	$2S + 1$	$\langle \hat{S}_z \rangle$	Energy	Iterations	Energy error	Variance	CSE norm
0	1	0	-2.180 965 69	20	6.6×10^{-7}	8.0×10^{-7}	4.3×10^{-8}
1	3	-1	-1.950 190 88	8	4.0×10^{-7}	4.1×10^{-7}	3.4×10^{-8}
2	3	0	-1.950 190 89	7	3.9×10^{-7}	5.2×10^{-7}	2.3×10^{-8}
3	3	1	-1.950 190 88	8	4.0×10^{-7}	4.1×10^{-7}	3.4×10^{-8}
4	3	-1	-1.736 546 45	13	6.4×10^{-7}	3.7×10^{-7}	3.9×10^{-8}
5	3	0	-1.736 545 43	9	1.7×10^{-6}	7.8×10^{-7}	3.9×10^{-8}
6	3	1	-1.736 546 45	13	6.4×10^{-6}	3.7×10^{-7}	3.9×10^{-8}
7	1	0	-1.667 110 63	17	8.6×10^{-7}	9.8×10^{-7}	6.5×10^{-8}
8	1	0	-1.638 926 31	9	4.1×10^{-7}	3.3×10^{-7}	2.0×10^{-8}
9	3	-1	-1.457 133 77	17	7.9×10^{-7}	6.0×10^{-7}	7.1×10^{-8}
10	3	0	-1.457 134 48	21	7.7×10^{-8}	9.5×10^{-7}	7.6×10^{-8}
11	3	1	-1.457 133 77	17	7.9×10^{-7}	6.0×10^{-7}	7.1×10^{-8}
12	1	0	-1.349 401 00	37	9.1×10^{-7}	8.6×10^{-7}	5.4×10^{-8}
13	3	-1	-1.303 974 95	37	9.8×10^{-6}	7.3×10^{-7}	6.4×10^{-8}
14	3	0	-1.303 984 43	11	2.8×10^{-7}	3.7×10^{-7}	2.2×10^{-8}
15	3	1	-1.303 971 02	39	1.4×10^{-5}	9.6×10^{-7}	1.0×10^{-7}

use a single high-spin Slater determinant, but when $\langle \hat{S}_z \rangle = 0$, unless noted otherwise, we use an equal linear combination of two determinants that are related by switching the α (spin up) and β (spin down) orbitals with the relative phases being $+1$ for a singlet and -1 for a triplet. Specific excited states are targeted by selecting particle-hole excitations from the Hartree-Fock ground state and, if necessary, spin adapting the excitations. Further control on the target states can be obtained by adding a second objective function to the optimization that biases the energy landscape towards a specific energy or energy range.

B. Results

The ground state and the first 15 excited states of linear H_4 as computed from the variance-based CQE are shown in Table II. The algorithm is performed iteratively until the energy variance is less than 10^{-6} a.u. The number of iterations required for convergence varies from 7 for the second-excited state to 39 for the fifteenth excited state. At convergence the energy error is also less than 10^{-6} hartrees except for the fifth, thirteenth, and fifteenth excited states. Even though the energies of the excited states need not be upper bounds to the energies from exact diagonalization, we find that all excited-state energies are strictly above those from diagonalization. We also compute the least-squares error in the CSE—the sum of the squares of the errors in the CSE, which is approximately an order of magnitude less than the energy variance for each state. For the fifth excited state, Fig. 2 shows the convergence of the energy error, variance, and least-squares CSE norm. We observe superlinear convergence toward zero in all three metrics for the error.

The energies of the ground state and the first three excited states of BH are shown as functions of the bond distance in Fig. 3. The solid lines denote the ground- and excited-state energies from exact diagonalization while the symbols denote the energies from the variance-based CQE. In each case the energy variance in the CQE is converged to less than

10^{-5} a.u. We observe that the CQE reproduces the potential-energy curves with maximum energy errors of 0.000 01, 0.000 08, 0.000 04, and 0.000 24 hartrees for the ground and first three excited states, respectively. Additional results from the BH calculations are available in the Supplemental Material [78].

The ground and first-three excited states of H_2 with $\langle \hat{S}_z \rangle = 0$ are computed. The five-qubit experiments were conducted with and without noise on fake-Lagos and state-vector quantum simulators in Qiskit, respectively. To demonstrate convergence, we consider the H_2 molecule at an internu-

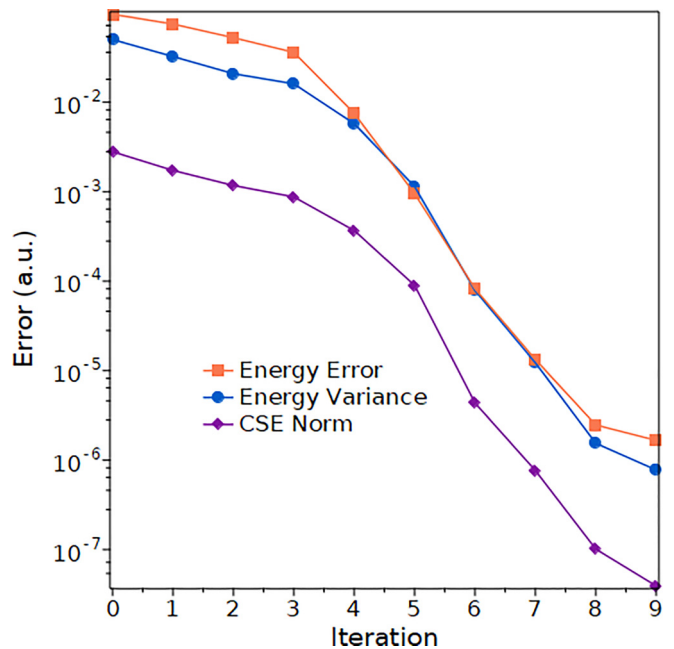


FIG. 2. Superlinear convergence of the energy error, variance, and least-squares CSE norm is shown for the fifth excited state of linear H_4 .

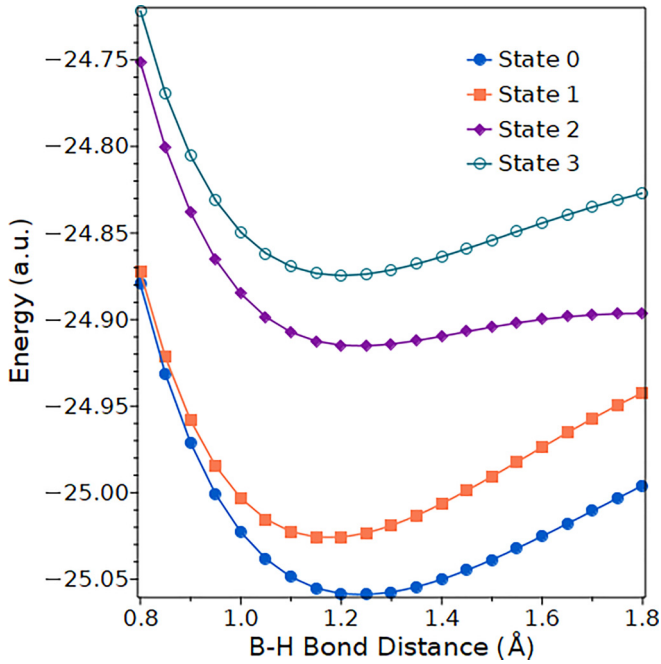


FIG. 3. Energies of the ground state and the first three excited states of BH are shown as functions of the bond distance. Symbols represent variance-based CQE energies while solid lines represent energies from exact diagonalization.

clear separation of 2.0 bohr. As shown in Fig. 4, using the state-vector simulator, we converge to the exact excited-state energy within 10^{-6} hartrees in less than 10 iterations; using the fake-Lagos simulator, we obtain the exact excited-state energy with an error of about 0.03 hartrees in about eight

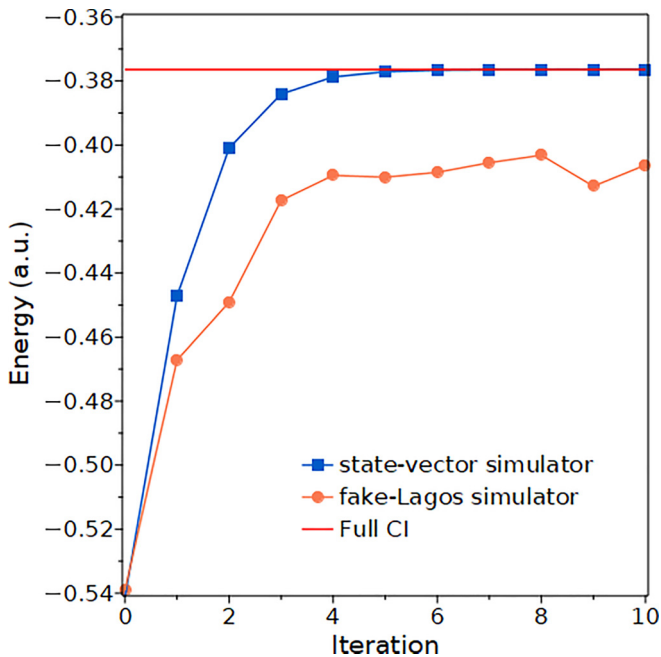


FIG. 4. The convergence of an excited-state energy of H_2 at 2.0 bohr on a quantum simulator with (fake-Lagos) and without (state-vector) noise.

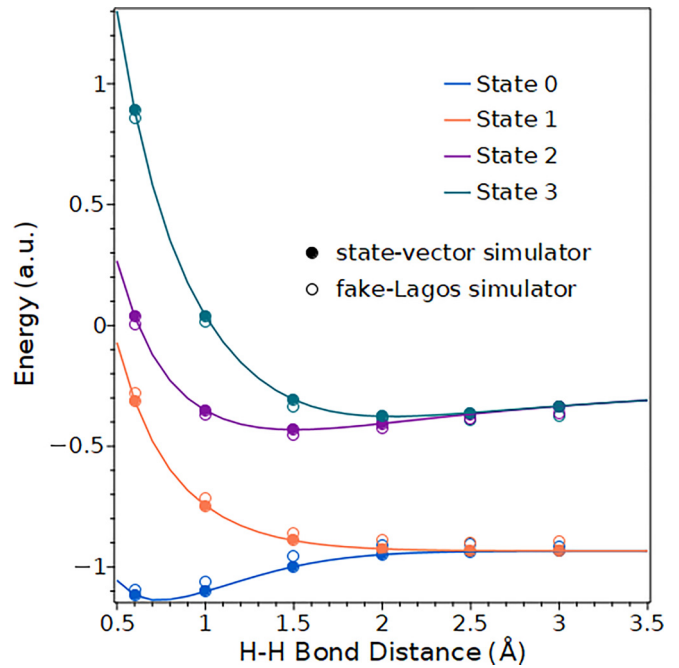


FIG. 5. The dissociation curves for the ground and first-three singlet excited states of H_2 are shown with (fake-Lagos) and without noise (state-vector).

iterations. For the first and second excited states we use single particle-hole excitations of the Hartree-Fock Slater determinant as initial guesses while for the third excited state we use a doubly excited Hartree-Fock Slater determinant. The dissociation curves of H_2 are shown in Fig. 5 with and without noise. The errors do not show significant differences for the various states, and they are also quite uniform throughout the dissociation. Additional results from the H_2 calculations are available in the Supplemental Material [78].

IV. CONCLUSIONS

Here we present a variance-based CQE for computing highly accurate molecular excited states on quantum computers. The CQE is a family of algorithms in which a contraction of the Schrödinger equation to the space of two particles (CSE) is solved for stationary-state energies and their 2-RDMs. The structure of the CSE implies an exact ansatz for any ground- or excited-state wave function in which a two-body exponential transformation is iteratively applied and optimized to update a trial wave function. Importantly, unlike iterative variational quantum eigensolvers, the CQE does not need to re-optimize previous transformations to satisfy the CSE and thereby solve the Schrödinger equation. While recent work with CQE has focused on the ground state, here we present a CQE algorithm for excited states in which we iteratively minimize the energy variance with respect to the CSE (or ACSE) ansatz. We show that the variance-based CQE yields highly accurate ground- and excited-state energies for the example cases of H_4 and BH in the absence of noise and H_2 in the presence of noise. Future work will examine the application of the variance-based CQE on noisy intermediate-scale quantum (NISQ) computers. The present

approach represents an important step towards the accurate modeling of molecular excited states on NISQ and fault-tolerant quantum computers.

Example notebooks of the code and calculations are available on Github [79].

ACKNOWLEDGMENTS

D.A.M. gratefully acknowledges the Department of Energy, Office of Basic Energy Sciences Grant DE-SC0019215, the U.S. National Science Foundation Grants No. CHE-2155082 and No. CHE-2035876.

- [1] V. W.-W. Yam, Using synthesis to steer excited states and their properties and functions, *Nat. Synth.* **2**, 94 (2023).
- [2] T. R. Nelson, S. Fernandez-Alberti, and S. Tretiak, Modeling excited-state molecular dynamics beyond the Born–Oppenheimer regime, *Nat. Comput. Sci.* **2**, 689 (2022).
- [3] Y. Wang, Y. Guan, H. Guo, and D. R. Yarkony, Enabling complete multichannel nonadiabatic dynamics: A global representation of the two-channel coupled, $1,2^1A$ and 1^3A states of NH_3 using neural networks, *J. Chem. Phys.* **154**, 094121 (2021).
- [4] J. E. Greenwald, J. Cameron, N. J. Findlay, T. Fu, S. Gunasekaran, P. J. Skabara, and L. Venkataraman, Highly nonlinear transport across single-molecule junctions via destructive quantum interference, *Nat. Nanotechnol.* **16**, 313 (2021).
- [5] L.-Y. Hsu, B.-Y. Jin, C.-H. Chen, and S.-M. Peng, Reaction: New insights into molecular electronics, *Chem* **3**, 378 (2017).
- [6] *Quantum Chemistry and Dynamics of Excited States*, edited by L. González and R. Lindh (Wiley, New York, 2021).
- [7] C. L. Benavides-Riveros, L. Chen, C. Schilling, S. Mantilla, and S. Pittalis, Excitations of Quantum Many-Body Systems via Purified Ensembles: A Unitary-Coupled-Cluster-Based Approach, *Phys. Rev. Lett.* **129**, 066401 (2022).
- [8] H. J. Monkhorst, Calculation of properties with the coupled-cluster method, *Int. J. Quantum Chem.* **12**, 421 (1977).
- [9] E. Runge and E. K. U. Gross, Density-Functional Theory for Time-Dependent Systems, *Phys. Rev. Lett.* **52**, 997 (1984).
- [10] J. F. Stanton and R. J. Bartlett, The equation of motion coupled-cluster method. a systematic biorthogonal approach to molecular excitation energies, transition probabilities, and excited state properties, *J. Chem. Phys.* **98**, 7029 (1993).
- [11] D. A. Mazziotti, Extraction of electronic excited states from the ground-state two-particle reduced density matrix, *Phys. Rev. A* **68**, 052501 (2003).
- [12] M. Casida and M. Huix-Rotllant, Progress in time-dependent density-functional theory, *Annu. Rev. Phys. Chem.* **63**, 287 (2012).
- [13] N. T. Maitra, F. Zhang, R. J. Cave, and K. Burke, Double excitations within time-dependent density functional theory linear response, *J. Chem. Phys.* **120**, 5932 (2004).
- [14] A. Dreuw and M. Head-Gordon, Failure of time-dependent density functional theory for long-range charge-transfer excited states: The zincbacteriochlorin-bacteriochlorin and bacteriochlorophyll-spheroidene complexes, *J. Am. Chem. Soc.* **126**, 4007 (2004).
- [15] D. Mester and M. Kállay, Charge-transfer excitations within density functional theory: How accurate are the most recommended approaches?, *J. Chem. Theory Comput.* **18**, 1646 (2022).
- [16] T. Moitra, L. Konecny, M. Kadek, A. Rubio, and M. Repisky, Accurate relativistic real-time time-dependent density functional theory for valence and core attosecond transient absorption spectroscopy, *J. Phys. Chem. Lett.* **14**, 1714 (2023).
- [17] J. Li, Y. Jin, N. Q. Su, and W. Yang, Combining localized orbital scaling correction and Bethe-Salpeter equation for accurate excitation energies., *J. Chem. Phys.* **156**, 154101 (2022).
- [18] J. W. Snyder and D. A. Mazziotti, Photoexcited conversion of gauche-1,3-butadiene to bicyclobutane via a conical intersection: Energies and reduced density matrices from the anti-Hermitian contracted Schrödinger equation, *J. Chem. Phys.* **135**, 024107 (2011).
- [19] Y. Wang and D. R. Yarkony, Conical intersection seams in spin-orbit coupled systems with an even number of electrons: A numerical study based on neural network fit surfaces, *J. Chem. Phys.* **155**, 174115 (2021).
- [20] K. Head-Marsden, J. Flick, C. J. Ciccarino, and P. Narang, Quantum information and algorithms for correlated quantum matter, *Chem. Rev. (Washington, DC, U.S.)* **121**, 3061 (2021).
- [21] K. Bharti, A. Cervera-Lierta, T. H. Kyaw, T. Haug, S. Alperin-Lea, A. Anand, M. Degroote, H. Heimonen, J. S. Kottmann, T. Menke, W.-K. Mok, S. Sim, L.-C. Kwek, and A. Aspuru-Guzik, Noisy intermediate-scale quantum algorithms, *Rev. Mod. Phys.* **94**, 015004 (2022).
- [22] S. Lloyd, A potentially realizable quantum computer, *Science* **261**, 1569 (1993).
- [23] Q. Gao, G. O. Jones, M. Motta, M. Sugawara, H. C. Watanabe, T. Kobayashi, E. Watanabe, Y.-Y. Ohnishi, H. Nakamura, and N. Yamamoto, Applications of quantum computing for investigations of electronic transitions in phenylsulfonyl-carbazole TADF emitters, *npj Comput. Mater.* **7**, 70 (2021).
- [24] A. Asthana, A. Kumar, V. Abraham, H. Grimsley, Y. Zhang, L. Cincio, S. Tretiak, P. A. Dub, S. E. Economou, E. Barnes, and N. J. Mayhall, Quantum self-consistent equation-of-motion method for computing molecular excitation energies, ionization potentials, and electron affinities on a quantum computer, *Chem. Sci.* **14**, 2405 (2023).
- [25] A. Kumar, A. Asthana, C. Masteran, E. F. Valeev, Y. Zhang, L. Cincio, S. Tretiak, and P. A. Dub, Quantum simulation of molecular electronic states with a transcorrelated Hamiltonian: Higher accuracy with fewer qubits, *J. Chem. Theory Comput.* **18**, 5312 (2022).
- [26] M. Q. Hlatshwayo, Y. Zhang, H. Wibowo, R. LaRose, D. Lacroix, and E. Litvinova, Simulating excited states of the Lipkin model on a quantum computer, *Phys. Rev. C* **106**, 024319 (2022).
- [27] Y. Kim and A. I. Krylov, Two algorithms for excited-states quantum solvers: Theory and application to EOM-UCCSD, *J. Phys. Chem. A* **127**, 6552 (2023).
- [28] J. R. McClean, M. E. Kimchi-Schwartz, J. Carter, and W. A. de Jong, Hybrid quantum-classical hierarchy for mitigation of decoherence and determination of excited states, *Phys. Rev. A* **95**, 042308 (2017).

- [29] J. I. Colless, V. V. Ramasesh, D. Dahlen, M. S. Blok, M. E. Kimchi-Schwartz, J. R. McClean, J. Carter, W. A. de Jong, and I. Siddiqi, Computation of Molecular Spectra on a Quantum Processor with an Error-Resilient Algorithm, *Phys. Rev. X* **8**, 011021 (2018).
- [30] K. M. Nakanishi, K. Mitarai, and K. Fujii, Subspace-search variational quantum eigensolver for excited states, *Phys. Rev. Res.* **1**, 033062 (2019).
- [31] T. Bian, D. Murphy, R. Xia, A. Daskin, and S. Kais, Quantum computing methods for electronic states of the water molecule, *Mol. Phys.* **117**, 2069 (2019).
- [32] O. Higgott, D. Wang, and S. Brierley, Variational quantum computation of excited states, *Quantum* **3**, 156 (2019).
- [33] M. Motta, C. Sun, A. T. K. Tan, M. J. O'Rourke, E. Ye, A. J. Minnich, F. G. S. L. Brandão, and G. K.-L. Chan, Determining eigenstates and thermal states on a quantum computer using quantum imaginary time evolution, *Nat. Phys.* **16**, 205 (2020).
- [34] J. R. McClean, Z. Jiang, N. C. Rubin, R. Babbush, and H. Neven, Decoding quantum errors with subspace expansions, *Nat. Commun.* **11**, 636 (2020).
- [35] T. Takeshita, N. C. Rubin, Z. Jiang, E. Lee, R. Babbush, and J. R. McClean, Increasing the Representation Accuracy of Quantum Simulations of Chemistry without Extra Quantum Resources, *Phys. Rev. X* **10**, 011004 (2020).
- [36] A. Francis, A. A. Agrawal, J. H. Howard, E. Kökcü, and A. F. Kemper, Subspace diagonalization on quantum computers using eigenvector continuation, [arXiv:2209.10571](https://arxiv.org/abs/2209.10571).
- [37] B. Huang, M. Govoni, and G. Galli, Simulating the electronic structure of spin defects on quantum computers, *PRX Quantum* **3**, 010339 (2022).
- [38] N. V. Tkachenko, Y. Zhang, L. Cincio, A. I. Boldyrev, S. Tretiak, and P. A. Dub, Quantum Davidson algorithm for excited states, [arXiv:2204.10741](https://arxiv.org/abs/2204.10741).
- [39] C. L. Cortes and S. K. Gray, Quantum Krylov subspace algorithms for ground- and excited-state energy estimation, *Phys. Rev. A* **105**, 022417 (2022).
- [40] Y. Shen, K. Klymko, J. Sud, D. B. Williams-Young, W. A. de Jong, and N. M. Tubman, Real-time Krylov theory for quantum computing algorithms, *Quantum* **7**, 1066 (2023).
- [41] N. Yoshioka, H. Hakoshima, Y. Matsuzaki, Y. Tokunaga, Y. Suzuki, and S. Endo, Generalized Quantum Subspace Expansion, *Phys. Rev. Lett.* **129**, 020502 (2022).
- [42] M. Motta, G. O. Jones, J. E. Rice, T. P. Gujarati, R. Sakuma, I. Liepuoniute, J. M. Garcia, and Y.-Y. Ohnishi, Quantum chemistry simulation of ground- and excited-state properties of the sulfonium cation on a superconducting quantum processor, *Chem. Sci.* **14**, 2915 (2023).
- [43] K. Kanno, M. Kohda, R. Imai, S. Koh, K. Mitarai, W. Mizukami, and Y. O. Nakagawa, Quantum-selected configuration Interaction: Classical diagonalization of Hamiltonians in subspaces selected by quantum computers, [arXiv:2302.11320](https://arxiv.org/abs/2302.11320).
- [44] S. Choi and A. F. Izmaylov, Measurement optimization techniques for excited electronic states in near-term quantum computing algorithms, *J. Chem. Theory Comput.* **19**, 3184 (2023).
- [45] D. A. Mazziotti, Contracted Schrödinger equation: Determining quantum energies and two-particle density matrices without wave functions, *Phys. Rev. A* **57**, 4219 (1998).
- [46] H. Nakatsuji and K. Yasuda, Direct Determination of the Quantum-Mechanical Density Matrix Using the Density Equation, *Phys. Rev. Lett.* **76**, 1039 (1996).
- [47] F. Colmenero and C. Valdemoro, Approximating q -order reduced density matrices in terms of the lower-order ones. II. applications, *Phys. Rev. A* **47**, 979 (1993).
- [48] D. A. Mazziotti, Anti-Hermitian Contracted Schrödinger Equation: Direct Determination of the Two-Electron Reduced Density Matrices of Many-Electron Molecules, *Phys. Rev. Lett.* **97**, 143002 (2006).
- [49] J.-N. Boyn and D. A. Mazziotti, Accurate singlet-triplet gaps in biradicals via the spin averaged anti-Hermitian contracted Schrödinger equation, *J. Chem. Phys.* **154**, 134103 (2021).
- [50] D. A. Mazziotti, Exactness of wave functions from two-body exponential transformations in many-body quantum theory, *Phys. Rev. A* **69**, 012507 (2004).
- [51] D. A. Mazziotti, Exact two-body expansion of the many-particle wave function, *Phys. Rev. A* **102**, 030802(R) (2020).
- [52] S. E. Smart and D. A. Mazziotti, Quantum Solver of Contracted Eigenvalue Equations for Scalable Molecular Simulations on Quantum Computing Devices, *Phys. Rev. Lett.* **126**, 070504 (2021).
- [53] J.-N. Boyn, A. O. Lykhin, S. E. Smart, L. Gagliardi, and D. A. Mazziotti, Quantum-classical hybrid algorithm for the simulation of all-electron correlation, *J. Chem. Phys.* **155**, 244106 (2021).
- [54] S. E. Smart and D. A. Mazziotti, Accelerated convergence of contracted quantum eigensolvers through a quasi-second-order, locally parameterized optimization, *J. Chem. Theory Comput.* **18**, 5286 (2022).
- [55] S. E. Smart, J.-N. Boyn, and D. A. Mazziotti, Resolving correlated states of benzyne with an error-mitigated contracted quantum eigensolver, *Phys. Rev. A* **105**, 022405 (2022).
- [56] S. E. Smart and D. A. Mazziotti, Many-fermion simulation from the contracted quantum eigensolver without fermionic encoding of the wave function, *Phys. Rev. A* **105**, 062424 (2022).
- [57] S. E. Smart and D. A. Mazziotti, Verifiably exact solution of the electronic Schrödinger equation on quantum devices, [arXiv:2303.00758](https://arxiv.org/abs/2303.00758).
- [58] J. R. McClean, J. Romero, R. Babbush, and A. Aspuru-Guzik, The theory of variational hybrid quantum-classical algorithms, *New J. Phys.* **18**, 023023 (2016).
- [59] F. Zhang, N. Gomes, Y. Yao, P. P. Orth, and T. Iadecola, Adaptive variational quantum eigensolvers for highly excited states, *Phys. Rev. B* **104**, 075159 (2021).
- [60] D.-B. Zhang, B.-L. Chen, Z.-H. Yuan, and T. Yin, Variational quantum eigensolvers by variance minimization, *Chin. Phys. B* **31**, 120301 (2022).
- [61] I. Hobday, P. Stevenson, and J. Benstead, Variance minimisation on a quantum computer for nuclear structure, [arXiv:2209.07820](https://arxiv.org/abs/2209.07820).
- [62] G. Boyd and B. Koczor, Training Variational Quantum Circuits with CoVaR: Covariance Root Finding with Classical Shadows, *Phys. Rev. X* **12**, 041022 (2022).
- [63] S. Liu, S.-X. Zhang, C.-Y. Hsieh, S. Zhang, and H. Yao, Probing many-body localization by excited-state variational quantum eigensolver, *Phys. Rev. B* **107**, 024204 (2023).

- [64] H. Nakatsuji, Equation for the direct determination of the density matrix, *Phys. Rev. A* **14**, 41 (1976).
- [65] D. A. Mazziotti, Multireference many-electron correlation energies from two-electron reduced density matrices computed by solving the anti-Hermitian contracted Schrödinger equation, *Phys. Rev. A* **76**, 052502 (2007).
- [66] D. A. Mazziotti, Anti-Hermitian part of the contracted Schrödinger equation for the direct calculation of two-electron reduced density matrices, *Phys. Rev. A* **75**, 022505 (2007).
- [67] G. Gidofalvi and D. A. Mazziotti, Direct calculation of excited-state electronic energies and two-electron reduced density matrices from the anti-Hermitian contracted Schrödinger equation, *Phys. Rev. A* **80**, 022507 (2009).
- [68] J. W. Snyder, A. E. Rothman, J. J. Foley, and D. A. Mazziotti, Conical intersections in triplet excited states of methylene from the anti-Hermitian contracted Schrödinger equation, *J. Chem. Phys.* **132**, 154109 (2010).
- [69] A. W. Schlimgen, K. Head-Marsden, Lee Ann M. Sager, P. Narang, and D. A. Mazziotti, Quantum Simulation of Open Quantum Systems Using a Unitary Decomposition of Operators, *Phys. Rev. Lett.* **127**, 270503 (2021).
- [70] K. Seki and S. Yunoki, Quantum power method by a superposition of time-evolved states, *PRX Quantum* **2**, 010333 (2021).
- [71] C. Miquel, J. P. Paz, M. Saraceno, E. Knill, R. Laflamme, and C. Negrevergne, Interpretation of tomography and spectroscopy as dual forms of quantum computation, *Nature (London)* **418**, 59 (2002).
- [72] H.-Y. Huang, R. Kueng, and J. Preskill, Predicting many properties of a quantum system from very few measurements, *Nat. Phys.* **16**, 1050 (2020).
- [73] D. C. Liu and J. Nocedal, On the limited memory BFGS method for large scale optimization, *Math. Program.* **45**, 503 (1989).
- [74] Qiskit contributors, Qiskit: An open-source framework for quantum computing (2023).
- [75] P. Jordan and E. Wigner, Über das Paulische Äquivalenzverbot, *Z. Phys.* **47**, 631 (1928).
- [76] W. J. Hehre, R. F. Stewart, and J. A. Pople, Self-consistent molecular-orbital methods. I. Use of Gaussian expansions of slater-type atomic orbitals, *J. Chem. Phys.* **51**, 2657 (1969).
- [77] RDMChem, Quantum Chemistry Toolbox in Maple (2023).
- [78] See Supplemental Material at <http://link.aps.org/supplemental/10.1103/PhysRevA.108.022814> for additional results from the BH and H₂ calculations such as the energy, number of iterations, the energy variance, and the norm of the CSE.
- [79] Example notebooks of the code and calculations are available on Github at <https://github.com/damaz/ExcitedState-CQE> (note that this material will be posted prior to publication).